

Attributing and Verifying European and National Greenhouse Gas and Aerosol Emissions and Reconciliation with Statistical Bottom-up Estimates

Deliverable 2.4
European CH_4 inversions

Authors: I. Cheliotis, S. Houweling, J. Thanwerdas, D. Brunner, M. Scholze, V. T. Manaparambil, Y. Villalobos

Date: 22/01/2026
Dissemination: Public
Work package: 2.4
Version: 1.0



This project has received funding from the European Union's Horizon Europe research and innovation programme under grant agreement No. 101081322

Views and opinions expressed are however those of the author(s) only and do not necessarily reflect those of the European Union or the Climate, Infrastructure and Environment Executive Agency (CINEA). Neither the European Union nor the granting authority can be held responsible for them.

Attributing and Verifying European and National Greenhouse Gas and Aerosol Emissions and Reconciliation with Statistical Bottom-up Estimates (AVENGERS)

Call: HORIZON-CL5-2022-D1-02

Topic: HORIZON-CL5-2022-D1-02-01

Type of action: HORIZON Research and Innovation Actions

Granting authority: European Climate, Infrastructure and Environment Executive Agency

Project starting date: 01/01/2023

Project end date: 31/12/2026

Project duration: 48 months

Contact: Dr. Marko Scholze, Coordinator

Lund University, Sweden

Document history:

Version	Author(s)	Date	Changes
Draft	I. Cheliotis, S. Houweling, VU	2025-11-05	1st version of the deliverable
Draft	I. Cheliotis, S. Houweling, VU	2025-12-18	Changes in the text and the plots
Draft	I. Cheliotis, S. Houweling, VU	2026-01-08	Additional text and plots
Draft	M. Scholze, V. T. Manaparambil, Y. Villalobos, LU	2026-01-10	Additional text
Draft	J. Thanwerdas, D. Brunner, EMPA	2026-01-13	Additional text
1.0	I. Cheliotis, S. Houweling, VU		Additional text and plots

Table of Contents

1 EXECUTIVE SUMMARY 4
2 INTRODUCTION 5
3 METHODOLOGY – PROTOCOL DESCRIPTION 5
4 INVERSION METHODS 9
4.1 WRF-CHEM CTDAS 9
4.1.1 Model description 9
4.1.2 WRF-CHEM CTDAS set-up for CH_4 9
4.2 ICON-ART CIF 10
4.2.1 Model description 10
4.2.2 ICON-ART CIF set up for CH_4 11
4.3 LUMIA 13
4.3.1 Model description 13
4.3.2 LUMIA set-up for CH_4 13
5 INVERSION RESULTS 13
6 DISCUSSION AND CONCLUSIONS 19
REFERENCES 21
APPENDIX 25

1 EXECUTIVE SUMMARY

The current report presents the results of an intercomparison for CH_4 inversions as simulated by three atmospheric inversion models, namely WRF-Chem CTDAS, ICON- ART CIF and LUMIA for the period 2010-2021. The analysis of the results revealed that the ICON-ART CIF model showcases the best performance out of the three with regards to the optimization of the CH_4 fluxes throughout the period under study. The ICON-ART CIF results where the least noisy and the model validation showcased a decrease of the RMSE of approximately 3ppb for the posterior mixing ratios compared to the prior with a negligible bias. WRF-Chem CTDAS was the least stable model with the results being quite noisy, especially for the posterior fluxes where the values vary in some cases more than 2Tgr/year for two consecutive months. The RMSE comparison for the validation stations showed an increase for the posterior mixing ratios compared to the prior for this inversion, indicating that the optimized fluxes do need lead to a general improvement in simulated mixing ratios. Regarding the LUMIA model, although it was less noisy than the WRF-Chem CTDAS model (country fluxes in some cases vary more than 1 Tgr/year between consecutive months), it showed an increase in the BIAS for the posterior mixing ratios of approx. 4 ppb compared to the prior. There were no data for the validation stations in the case of LUMIA. Another noteworthy result was the decrease of the CH4 fluxes of approx. 1 to 3Tgr/year in the ensemble of the European Union countries from the year 2010 compared to 2021, as displayed by all 3 models for the prior as well as the posterior runs. Focusing on the region of Benelux we notice some positive systematic emission adjustments in the fluxes difference between the posterior and the prior runs for ICON-ART CIF and LUMIA. Further investigation in the seasonal cycle for Benelux as simulated by ICON-ART CIF revealed that the enhancements appeared in all the twelve months with the maximum values observed in January, February, June and July exceeding 0.6Tgr/year and the minimum values in April and May approx. 0.4Tgr/year. On the other hand, WRF-Chem CTDAS showcased a dipole of positive emission adjustments around the two stations in the Netherlands (Cabauw and Lutjewad) and negative adjustments in the rest of the country. By investigating further the results from the three models for the two stations, we noticed an increase of the CH_4 mixing ratios reaching approx. 0.02ppb or higher for the two stations. Overall, the analysis of the results from the three models showed that the ICON-ART CIF model not only had the best performance for the validation, but it was also more consistent with the previous findings in similar studies for Europe. WRF-Chem CTDAS and LUMIA present some deviations compared to previous studies, as well as in some cases worse performance of the posterior results compared to the prior as revealed by the models' validation.

2 INTRODUCTION

An improved quantification of CH_4 emissions, by region and emission sector, is crucial as it is the second most important anthropogenic greenhouse gas after CO_2 (Myhre, et al, 2014). During the industrial era CH_4 emissions have more than doubled (Dalsøren et al, 2016) with a 20% increase in the past two decades. Furthermore, the anthropogenic emissions account for 60% of the total CH_4 emissions and the observed CH4 concentrations follow a pessimistic IPCC trend leading to a global temperature increase above 3°C by the end of the century (Jackson et al, 2024). The combined European union countries rank in the top six world GHG emitters among China, USA, India, Russia and Indonesia (Crippa et al, 2025). The lifecycle of CH_4 is approximately 9 years (Prather et al, 2012), therefore mitigation measures for the reduction of CH_4 emissions will have a faster response in the atmosphere compared to CO_2 with its' much longer lifetime (Shindell et al, 2012).

The current report contributes to the AVENGERS project by providing the results for 12 years (2010-2021) of CH_4 simulations over Europe using three different atmospheric inversion model set-ups, these are the WRF-Chem CTDAS, ICON-ART CIF and LUMIA. The aim is to investigate the long-term trends of CH_4 fluxes over Europe. More particularly, we estimate the uncertainty range of inversion-optimised CH_4 emissions and examine its' year-to-year changes and the long-term trend. In addition, we formulate guidelines and best practices for atmospheric inversion setups that can be used by non-scientific parties.

This report presents an analytical description of the methodology and the protocol used by the three model set-ups (Chapter 3. The results from the CH_4 inversions and the inter-comparison between the models is presented in Chapter 4 followed by the discussion and conclusions in Chapter 6.

3 METHODOLOGY – PROTOCOL DESCRIPTION

The experiment consists of atmospheric CH_4 inversions covering the period 2010-2021. The aim is to estimate the CH_4 emissions and emission trends that are consistent with the available surface measurements from the European Integrated Carbon Observation System (ICOS). The results are used to assess the performance of atmospheric inverse modelling techniques, the atmospheric transport models that are used, and the constraints they provide on inventory estimates of national emissions. The Swiss Federal Laboratories for Materials Science and Technology (EMPA) and Lund University groups extended the inversions up to 2023. The regional inversions cover at minimum the area from 15°W to 35°E and 35°N to 72°N with minor differences between the groups depending on the transport models and the preferred spatial resolutions.

The CH_4 fluxes were assigned to the models with the anthropogenic and the natural fluxes as two separate categories. For the anthropogenic category, the data were taken from the TNO inventory (Kuenen et al, 2014) with updates for some countries (Germany, Italy, the Netherlands, Switzerland) represented by inventory experts in the AVENGERS consortium. For the natural category, the data were taken from different inventories, more specifically the Global Fire emissions Database (GFED 4.1; Randerson et al, 2018) was selected for the fire emissions, the Lund-Potsdam-Jena General Ecosystem Simulator output (LPJ-GUESS; Nord et al, 2021) for the wetlands and the rest of the natural emissions from the Global Methane Budget report (termites, ocean and freshwater; Saunois et al, 2020). It is important to note that there was some overlap between the TNO data and GFED regarding the wildfires, hence eventually only the wildfires from the GFED dataset were used.

For the optimization of the CH_4 emissions, in-situ surface observations from the ICOS network were used. The stations were divided between mountain (only nighttime observations-00:00 and 06:00 local time) and the rest of the stations (only daytime observations-12:00 local time) to avoid daytime upslope winds and a shallow boundary layer respectively (Steiner et al, 2024). The prescribed observational uncertainty for each station was chosen by the groups based on their models. The complete list of the stations is presented in Appendix in Table 1. The periods with available data differ between the stations and therefore some stations were eventually not used for some periods in the optimization or validation. Figure 1 provides the overview for the data availability for each station.

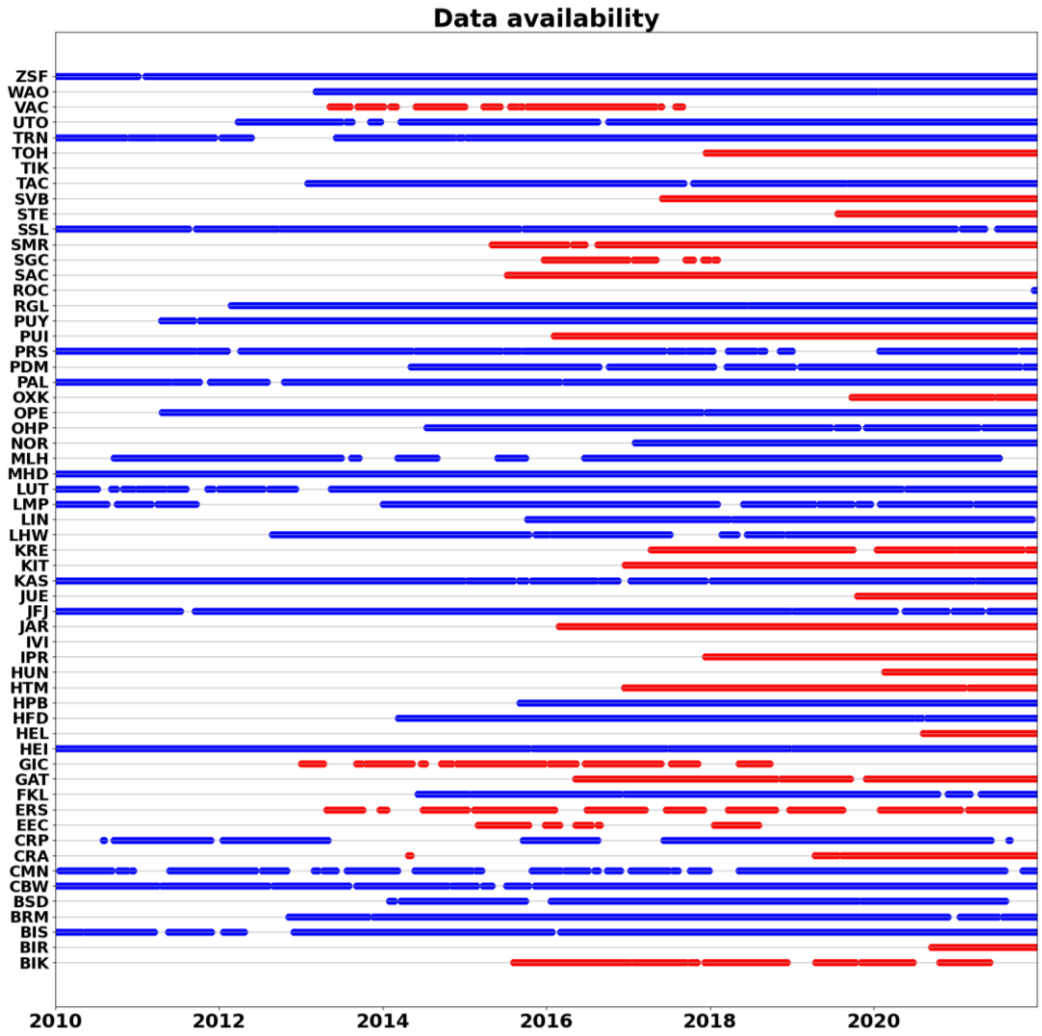


Figure 1: Data availability for the optimization (blue) and validation (red) stations used in the simulations.

The domain as used in WRF-CTDAS and the locations of the optimization (blue) and validation (red) stations are displayed in Figure 2.

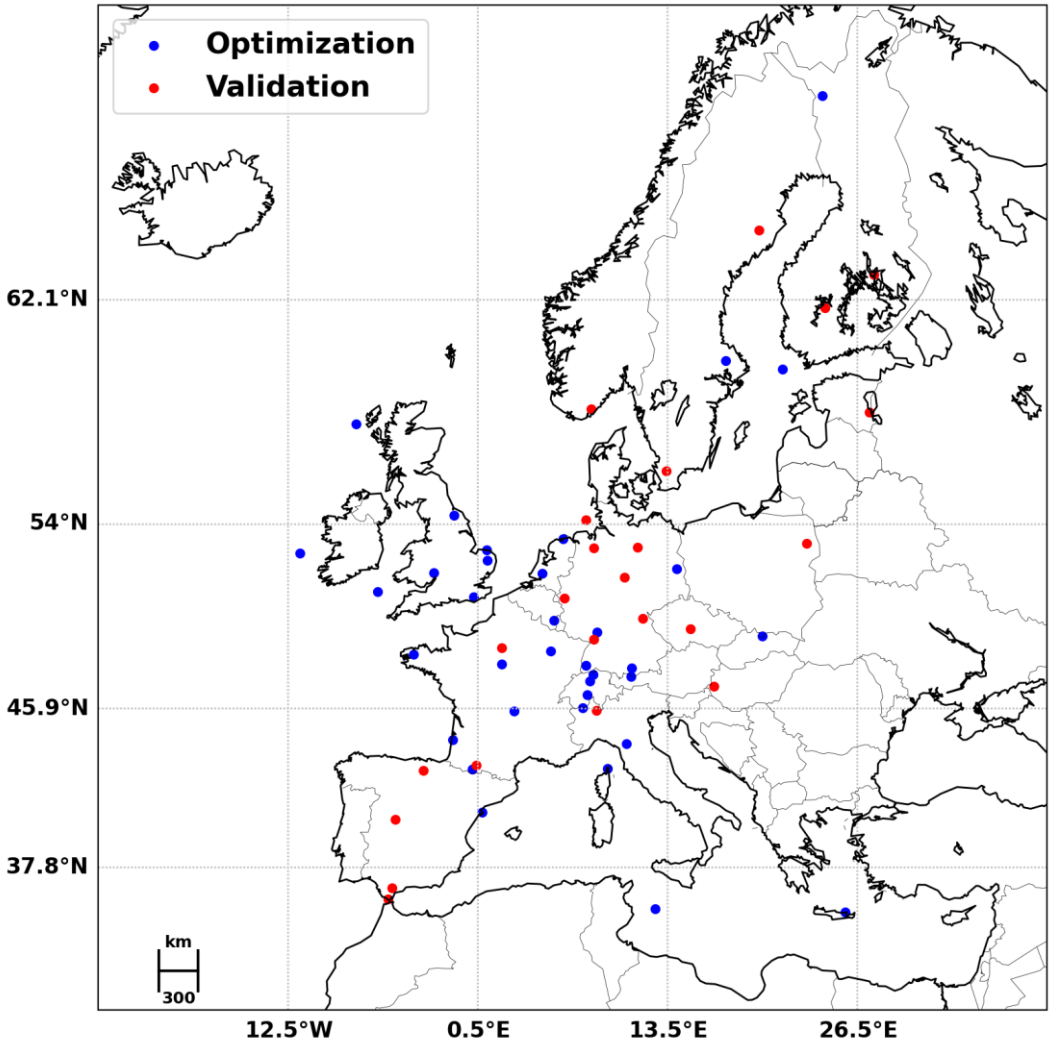


Figure 2: Domain of the CH4 simulations along with the locations for the optimization (blue) and the validation (red) stations

The ERA5 reanalysis dataset was used to provide meteorological fields to the offline transport model LUMIA as well as a meteorological nudging for the online ICON-ART and WRF-Chem models (Hersbach et al, 2018). For the background/boundary conditions of the CH_4 mixing ratios, the Copernicus Atmospheric Service (CAMS; Kuenen et al, 2022) data version 22 r1 was used.

All the groups provided the model outputs in a common format including the prior and the posterior mixing ratios for the stations and their uncertainties, the prior and the posterior fluxes per grid cell, as well as per country separately for the anthropogenic and the natural categories. The detailed description of the models and the inversion set-ups operated for this study are presented in Chapter 4.

4 Inversion methods

4.1 WRF-CHEM CTDAS

4.1.1 Model description

Partner VUA used the atmospheric chemistry model WRF-Chem, version 4.5.2 (Drell et al, 2005) for simulating the CH_4 mixing ratios over Europe. The WRF-Chem model has the ability to simulate gases acting as either passive tracers or including the chemical reactions. The first option was chosen for this study, motivated by the long lifetime of CH_4 compared to the relevant transport timescales in the domain that is used. The spatial resolution was 25 by 25 km with a time step of 6 hours. For the domain of Figure 2 this spatial resolution translates to 191 grid points in the west-east direction and 171 grid points in the south-north direction. Since the spatial resolutions of the different inventories vary and they are different from the model, it was necessary to regrid the emissions to the 25 by 25km resolution. For this part, the Swiss Federal Laboratories for Material Science and Technology (EMPA) assisted us with a sophisticated code, namely the emiproc, used to regrid the emissions from the different inventories in the correct spatial resolution in a mass conserving manner (for details see Jähn et al, 2020). A model integration time step of 150 seconds was selected. WRF-Chem was run with 38 vertical eta levels (up to 20 km height) with all the emissions assigned to the first (surface) level, without the use of nested subdomains. The spectral nudging option was enabled in order to constrain the WRF computed dynamics to the ERA-5 reanalysis. Other noteworthy parameters in the WRF-Chem are the MYJ planetary boundary layer scheme and the Morrison 2-moment microphysics scheme. Additional tracers needed for ensemble simulations were added in one of the GHG chemistry packages already existing in the WRF-Chem registry. Appendix Table 2 summarizes the WRF-Chem set up used in WRF-CTDAS.

4.1.2 WRF-CHEM CTDAS set-up for CH_4

The CH_4 emissions were optimized by the CarbonTracker Data Assimilation Shell (CTDAS; van der Laan-Luijkx et al, 2017) using the ensemble Kalman smoother technique (Peters et al, 2005). This method represents the statistics of the inverse problem by a set of ensemble members acting as tracers in the simulation. Combining the ensemble members, their means and the corresponding observations, the CTDAS estimates the scaling factors which consequently optimize the emissions, updating the first guess. A new cycle starts for the simulation of the next time window with the newly optimized emissions as inputs. The CTDAS was coupled with the WRF-Chem for several gases by Reum et al (2021). Ioannidis et al (2025) have demonstrated the performance of the WRF-Chem CTDAS regarding CH_4 emissions over Europe. For the current work a similar set-up was implemented.

Due to the structure of the model, we had to carry out two separate runs, one with the inversion enabled (optimized/posterior emissions) and one with the inversions disabled (prior emissions-forward run) in order to evaluate the performance of the inversions. We selected 60 ensemble members with two cycles of 10 days each leading to a total of 20 days assimilation window length. In addition to the optimization of the emissions, we implemented the optimization of the fluxes of the boundary conditions thus leading in the total amount of 16158 scaling factors. We acknowledge that the number of the ensemble members is not optimal for our domain. The selection of 150 ensemble members or more would be more fitting, as Thanwerdas et al (2025) have demonstrated. However, the time and computational limitations led us to the decision of a smaller ensemble. The domain was split in regions with each region containing 4 grid cells, meaning if the observation station is located within this region, it will optimize the whole region without resolving the grid cell in which the station is located. The spatial error correlation length scale was set to 300km in combination with a localization length of 900km. This means that the grid cell aggregation in the state vector is well within the flux correlation length scale. The localization length causes multiple state vector elements to be addressed by measurement information from each site in the network. The amount of input data needed to run the model was substantial and therefore we divided the 2010-2021 period in annual inversions computed in parallel. The most noteworthy CTDAS options are included in Table 2.

4.2 ICON-ART CIF

4.2.1 Model description

EMPA carried out the simulations by using the inversion the Icosahedral Nonhydrostatic (ICON) weather and climate model (Zängl et al., 2015) coupled with the Community Inversion Framework (CIF; Berchet et al., 2021). ICON is a collaborative effort between the Deutscher Wetterdienst (DWD), the Max Planck Institute for Meteorology (MPI-M), the Deutsches Klimarechenzentrum (DKRZ), the Karlsruhe Institute of Technology (KIT), and the Center for Climate Systems Modeling (C2SM) in Switzerland. Its goal is to develop a unified, next-generation global system for numerical weather prediction (NWP) and climate modeling. ICON became operational within DWD's and MeteoSwiss' forecasting systems in 2015 and 2024, respectively. Notably, ICON was made available as open-source software to expand its user and developer community in February 2024. To incorporate atmospheric chemistry and aerosol processes, ICON is extended by the Aerosols and Reactive Trace gases (ART) module, developed and maintained by KIT (Hoshyaripour et al., 2025; Schröter et al., 2018; Rieger et al., 2015). This combination forms the ICON-ART model, a non-hydrostatic Eulerian chemical transport model that includes emissions, transport, gas-phase chemistry, and aerosol dynamics in both the troposphere and stratosphere. ICON-ART uses an icosahedral grid that can cover the entire globe or be restricted to limited areas, ranging in horizontal resolution from several degrees down to a few kilometers.

CIF is a system that has been designed to bring together the different inversion methods (analytical, variational and ensemble) and transport models used in the inversion community. It is built as an open-source, well documented, highly modular multi-model inversion framework written in Python that facilitates the comparison of (1) inversion methods and (2) transport models. CIF has proved to be accurate and computationally performant over the past years (Wittig et al., 2023; Savas et al., 2023; Remaud et al., 2022; Thanwerdas et al., 2024, 2022b,a).

The ensemble square root filter (EnSRF) algorithm is implemented in CIF to perform the inversions presented in this study. This algorithm has recently been improved and is thoroughly described in Thanwerdas et al. (2025). Briefly, an ensemble of vectors is used to represent the probability distribution of the state vector (also called control vector), which contains all the variables that we wish to optimize (e.g., fluxes, background concentrations, etc). Each member of the ensemble is attached to a different tracer transported by the model. After running simulations with this ensemble of tracers, the resulting ensemble of output concentrations is used to optimize the state vector to minimize the mismatch with the assimilated observations of atmospheric concentrations.

4.2.2 ICON-ART CIF set up for CH_4

For the present study, the model is configured with a horizontal resolution of 26km (approximately 0.3°) over Europe (15°E – 35°E, 33°N – 73°N), consisting of 21,344 grid cells. Vertically, the model extends from the surface up to 23km with 60 levels, using a height-based, terrain following coordinate system. Meteorological variables are computed online by the ICON model. Key prognostic variables (including wind speed, specific humidity, density, virtual potential temperature, and Exner pressure), are weakly nudged toward ERA5 reanalysis data (Hersbach et al., 2023, 2018) from the ECMWF, available at a 3-hourly temporal resolution. This nudging helps maintain the model's realism and prevents significant drift from observed atmospheric conditions. ERA5 data also provide the model's initial state. Emission fields for transported species are processed via the Online Emissions Module (OEM; Jähn et al., 2020), integrated within ART. Output files of instantaneous concentrations are saved hourly and later interpolated in time, height, and space to derive model equivalents of observational data.

We independently optimize two categories of CH_4 emissions: anthropogenic and natural emissions. In addition, we optimize both the background CH_4 concentrations (defining the initial atmospheric state at the start of the simulation), and the boundary inflow conditions (representing CH_4 transported into the regional domain from external regions).

Emission fluxes are optimized at the level of individual grid cells across the horizontal domain. Background concentrations are optimized across 32 inflow regions. They are defined as radial sectors, each covering an equal angular region centered on the midpoint of the domain's latitude–longitude extent. Initial concentrations are optimized using the full extent of the 32 regions, whereas boundary concentrations throughout the simulation are optimized along the domain borders only.

The full assimilation period is partitioned into consecutive 10-day windows. Within each window, a single scaling factor is assigned to every optimized variable. The scaling factors are optimized using observations from both the current window and the subsequent window (i.e., the number of lags is set to 2). To suppress spurious long-range correlations within the ensemble, covariance localization is applied using an exponential decay function with a characteristic decay length of 600 km, following the recommendations of Thanwerdas et al. (2025).

To reduce the total runtime, each year is inverted independently, preceded by a one-month spin-up and followed by a one-month spin-down.

Uncertainties in both the prior information and the observations are represented through covariance matrices, which quantify the assumed statistical relationships between optimized variables. The prior-error covariance matrix characterizes uncertainties in the a priori flux estimates, while the observation-error covariance matrix accounts for uncertainties in the assimilated measurements and in the modeled atmospheric transport. All errors are assumed to follow a normal (Gaussian) probability distribution.

For the scaling factors associated with surface fluxes, we prescribe a relative standard deviation of 100 % (square-root of diagonal elements of the covariance matrix). Spatial correlations are represented through a correlation matrix constructed using an exponential decay function. These correlations are then multiplied by the corresponding variances to form the off-diagonal elements of the covariance matrix.

Szénási et al. (2021) estimated correlation lengths of 100–150 km for agricultural methane emissions, while assuming negligible spatial correlation for non-agricultural sources. These findings suggest that realistic correlation lengths for anthropogenic emissions are relatively short, generally below 100 km. However, adopting such small values in our inversion framework would substantially limit the number of effective observational constraints, given the sparse spatial coverage of assimilated measurements. Moreover, for consistency and comparability with previous studies, we adopt intermediate correlation lengths, defined as follows:

- 150 km for anthropogenic emissions
- 200 km for natural emissions

For the scaling factors associated with background concentrations, we use a relative variance of 0.5 % (~ 10 ppb) and a large-scale correlation length of approximately 2000 km, following the value estimated by Szénási et al. (2021). We also apply temporal correlations with exponential decays of 3 months to emissions and background concentrations.

The observation error is computed based on a series of forward and inverse simulations. We first perform a forward simulation for all the years. Simulated values are then sampled and compared to observations to compute an initial estimate of observation error using the root mean square error (RMSE). This estimate is used to perform a first inversion for the period 2010-2023. Following the inversion, we recalculate the RMSE, which serves as a refined estimate of the observation error for these stations.

4.3 LUMIA

4.3.1 Model description

The simulations for the third inversion system was carried out by the Lund university using the Lund University Modular Inversion Algorithm (LUMIA, Monteil and SCholze, 2021). LUMIA relies on the atmospheric transport model FLEXPART (version 11) to compute CH_4 transport. It is a Lagrangian particle dispersion model and it computes dispersion of virtual air "particles", backward in time, based on meteorological fields from ECMWF ERA5 data. FLEXPART will provide the "footprints" of the CH4 observations, which is the sensitivity of each observations to the surface fluxes. The footprints are calculated at a horizontal resolution of 0.25°, for a regional domain ranging from 15°W, 33°N to 35°E, 72°N. The background concentrations are estimated from the CAMS CH_4 concentration products using the final position of the particles (latitude, longitude, time, height above ground level).

4.3.2 LUMIA set-up for CH_4

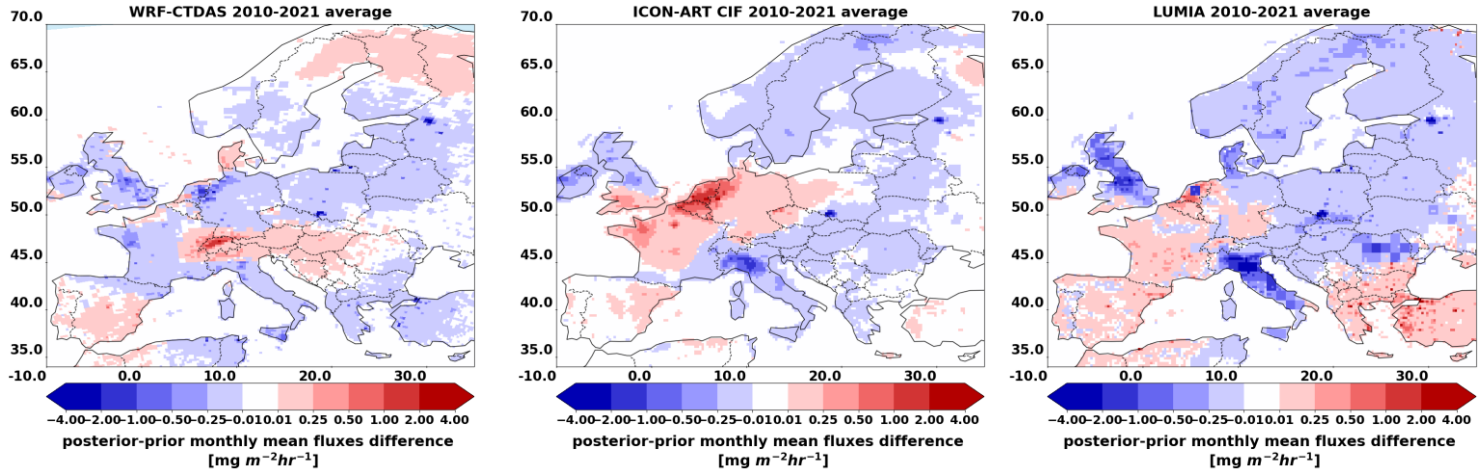
The CH_4 fluxes were divided into anthropogenic, wetlands and natural categories for optimization. The gridded anthropogenic emissions from TNO were used as the prior for the anthropogenic category. Prior emission fields for wetland emissions were taken from the LPJ-GUESS. Natural category is created by combining geological, ocean, termites, freshwater and biomass burning components from the global methane budget report in the same manner as in the case of WRF-CTDAS and ICON-ART CIF. Spatio-temporal correlations for the prior uncertainties were defined using exponential decay functions, with correlation lengths of 500km and 30 days for the anthropogenic fluxes, 5000km and 1000 days for natural fluxes and 1000km and 30 days for wetlands. All these three flux categories have been optimized at daily interval.

5 Inversion results

All the participating groups carried out the CH_4 inversions implementing the protocol described in Section 3 for the entire period 2010-2021. In addition, the CIF-ICON ART and the LUMIA models extended the simulations for the years 2022-2023. By analysing the difference between the fluxes before and after the optimization for the whole domain, the information on methane emissions in the ICOS measurements is assessed. In Figure 3, we display the posterior-prior flux differences averaged for the period 2010-2021 for the three models. Some similarities between the models show up, such as negative values in most of the United Kingdom and Eastern Europe. For WRF-CTDAS and ICON-ART CIF, the emission adjustments range between -0.01 and -0.5mg.m^{-2}.hour^{-1}, whereas the LUMIA values are a bit higher exceeding -1mg.m^{-2}.hour^{-1}. The ICON-ART CIF and LUMIA models also show similar patterns

in North Italy, with negative adjustments ranging mainly from -1 to -2 mg.m^{-2}.hour^{-1}. The LUMIA results also show larger differences in this case, exceeding -2 mg.m^{-2}.hour^{-1} with negative adjustments extending to mid and southern Italy. On the other hand, WRF-CTDAS shows a positive pattern in North Italy with the core of the pattern appearing in Switzerland reaching 2 mg.m^{-2}.hour^{-1}.

Another interesting area to observe is the Netherlands. ICON-ART CIF model shows a positive adjustment throughout the Benelux area with upward flux corrections exceeding 2 mg.m^{-2}.hour^{-1}. LUMIA also shows positive adjustments in the Benelux area except a box area of negative values in the middle of the Netherlands, calling for further investigation. The WRF-CTDAS shows positive emission adjustments in The Netherlands only around the Cabauw and Lutjewad stations compensated by negative adjustments elsewhere in The Netherlands. Ioannidis et al (2025) also found a strong dipole of positive emission adjustments in nothern Netherlands contrasted by negative values in the south of the country in WRF-CTDAS estimated posterior-prior fluxes difference for the years 2008, 2013 and 2018. In their study only the north station (Lutjewad) was used in the optimization. This could indicate that the flux optimization in WRF-CTDAS remains local despite the selection of the correlation and localization lengths covering much larger distances.



a b c

Figure 3: Posterior-prior monthly mean fluxes difference averaged for the period 2010-2021 for WRF-Chem CTDAS (a), ICON-ART CIF (b) and LUMIA (c).

Next we analyze temporal variations in flux adjustments to evaluate trends in the (a priori) emissions inventory against atmospheric measurements. To do this, we sum of the monthly mean prior and posterior fluxes separately for subregions such as the 27 European Union countries and the Benelux area across the period 2010-2021 for the three models. The results are presented in Figure 4 and in more details per month in Figure 8 in Appendix. It is evident that the ICON-ART CIF estimated emissions remains closest to the prior, followed by the LUMIA model. WRF-CTDAS shows a large variation in the posterior fluxes with values fluctuating up to 20Tgr/year from one month to another. The a priori emissions show temporal patterns that is very similar between the years in all three models. All three models show a small decline of approximately 1 to 3Tgr/year for both the prior and the posterior fluxes of the European Union from January 2010 to the December 2021. The corresponding results for the Benelux countries show a decline in the prior fluxes for the WRF-CTDAS (with

large fluctuations) and LUMIA inversions of approximately 0.2-0.3Tgr/year from January 2010 to December 2021 with the posterior fluxes also showing an overall decline although the values fluctuate from year to year showing secondary maximums in the years 2011, 2015 and 2019 and minimums in 2014 and 2017. On the contrary, the prior fluxes in ICON-ART CIF in the Benelux area are stable throughout the period, whereas the posterior fluxes show an increase from 2010 to 2015 of approximately 0.3Tgr/year followed by a slight decline until 2021.

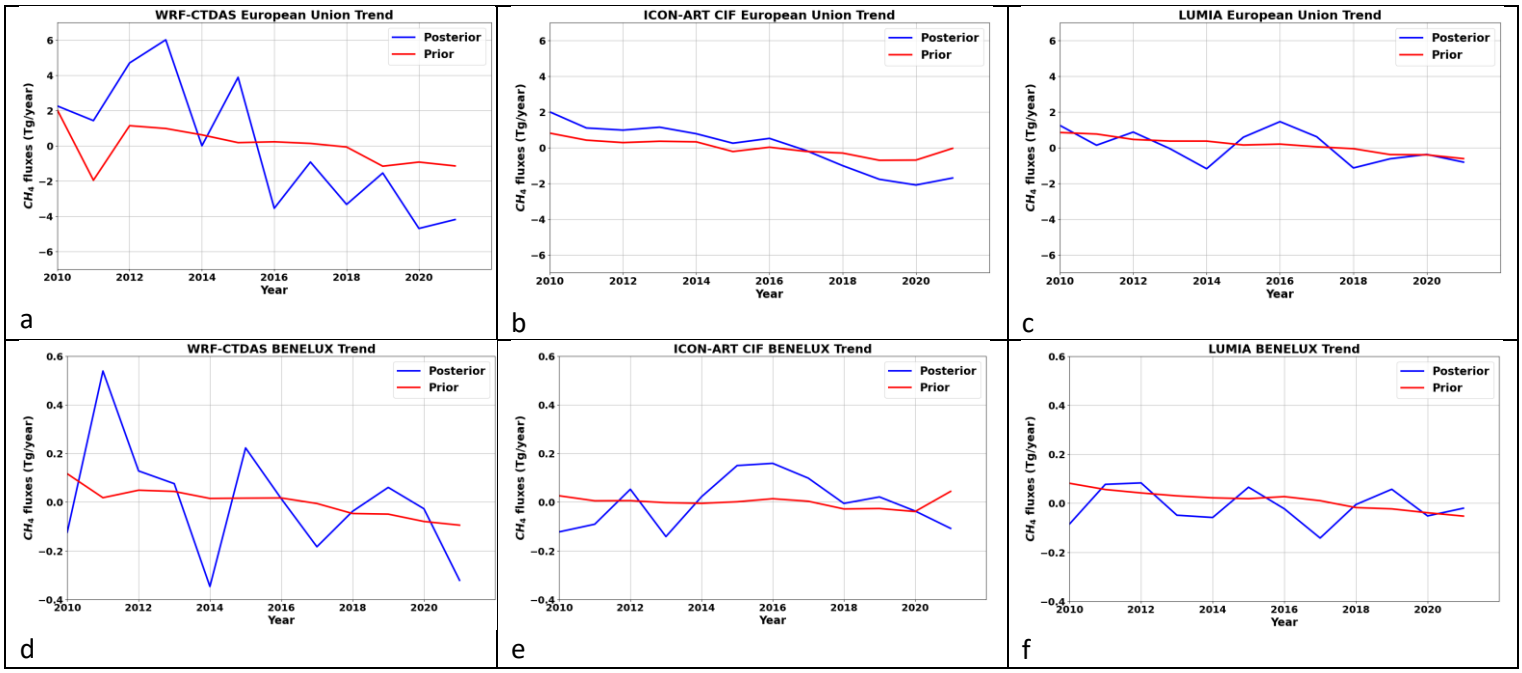


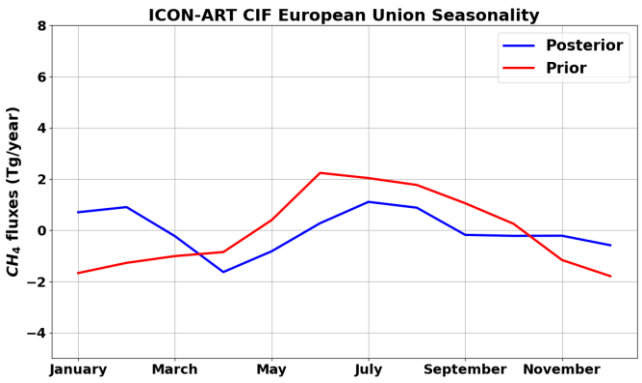
Figure 4: Monthly mean prior and posterior fluxes for the period 2010-2021 for the sum of the European Union countries (WRF-CTDAS (a), ICON-ART CIF (b) and LUMIA (c)) and the Benelux countries (WRF-CTDAS (d), ICON-ART CIF (e) and LUMIA (f)) averaged for every year.

As already presented in Figure 3, the values for the posterior fluxes are higher than the prior fluxes in Benelux area for the ICON-ART CIF model. In Figure 8e, we can see that this is true almost for the entire period January 2010-December 2021 with the difference exceeding even 1.5Tgr/year in some cases. In other words, the current emissions inventories significantly underestimate the emissions systematically for the period 2010-2021. In order to investigate further these differences we prepared plots of the seasonal cycles of the CH_4 fluxes, displayed in Figure 5. More particularly, we estimated the mean of the fluxes for each month from the 12 year period 2010-2021 for the EU and Benelux for the ICON-ART CIF and the LUMIA models. For the EU, the maximum values for the prior and posterior fluxes are observed during the months of July/August with the minimum found during April and December in the case of ICON-ART CIF. The amplitude in this case is approx. 3Tgr/year. This is similar to the results from Ioannidis et al study (2025) regarding the seasonal cycle for EU. On the other hand, in LUMIA although the maximum and minimum values for the prior fluxes are also in agreement with ICON-ART CIF and Ioannidis et al study with the amplitude in this case being approx. 4Tgr/year, the posterior fluxes show the exact opposite behavior. The maximum values are found in March and April with the minimum values in June and July and the amplitude in this case is approx. 10 Tgr/year.

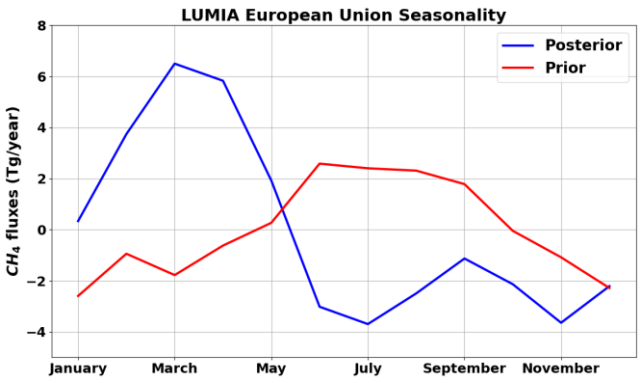
For the Benelux region, in the ICON-ART CIF results, we observe a decline from April until September exceeding 0.1Tgr/year for the prior emissions. The results from LUMIA in the same region also show a similar decline, nevertheless the results fluctuate slightly in this case. In the study of Ioannidis et al (2015), we see similar seasonal cycles in the plot for the Western European countries. Regarding the posterior emissions, in LUMIA results, there is also a decline between April and September but the amplitude in this case exceeds 0.4Tgr/year. In ICON-ART CIF, the posterior emissions show a different behavior regarding the seasonality, with a maximum in February and a decline in March with the minimum in April resulting to a difference that exceeds 0.3Tgr/year compared to February. Consequently, there is an increase that continues until July with the difference compared to April being slightly less than 0.3Tgr/year the declines and increase continue from Septmber until December.

Figure 5 showcases the values after subtracting the mean, so the prior and posterior results can be comparable. In Appendix we included displaying the prior and posterior emissions without subtracting the mean in order to observe the enhancements differences throughtout the months. For the EU, the posterior fluxes show an enhanced seasonal cycle for both models until March, with the enhancement continuing for LUMIA model until April of approx. 0.2Tgr/year for ICON-ART CIF and more than 0.5 Tgr/year for LUMIA. From May until October the prior emissions are higher compared to the posterior by approx. 2Tgr/year for ICON-ART CIF and by almost 10 Tgr/year for LUMIA.

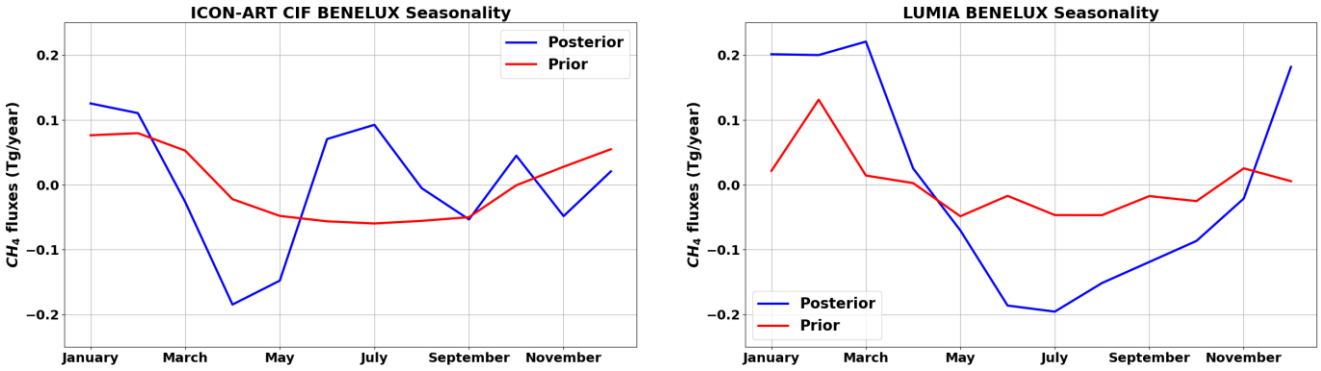
For Benelux, in the ICON-ART CIF results we see strong enhancements for all the months. The higher differences are observed during the months with maximum values, namely January, February, June and July. In these cases the enhancements exceeded 0.6Tgr/year. The minimum enhancements are found in April and May but neverthless they are approx. 0.4Tgr/year. LUMIA results show enhancements during the months of January, February, March, April, May, November and December with the highest enhancement observed in January and March with the values exceeding 0.2Tgr/year and the minimum enhancement found in November with the posterior fluxes being barely higher than the prior. During the months of June, July, August and September, the prior emissions are higher with the larger difference of approx. 0.1Tgr/year in June. This outcome is most likely connected to the box of negative adjustments we have seen in Figure 3.



a



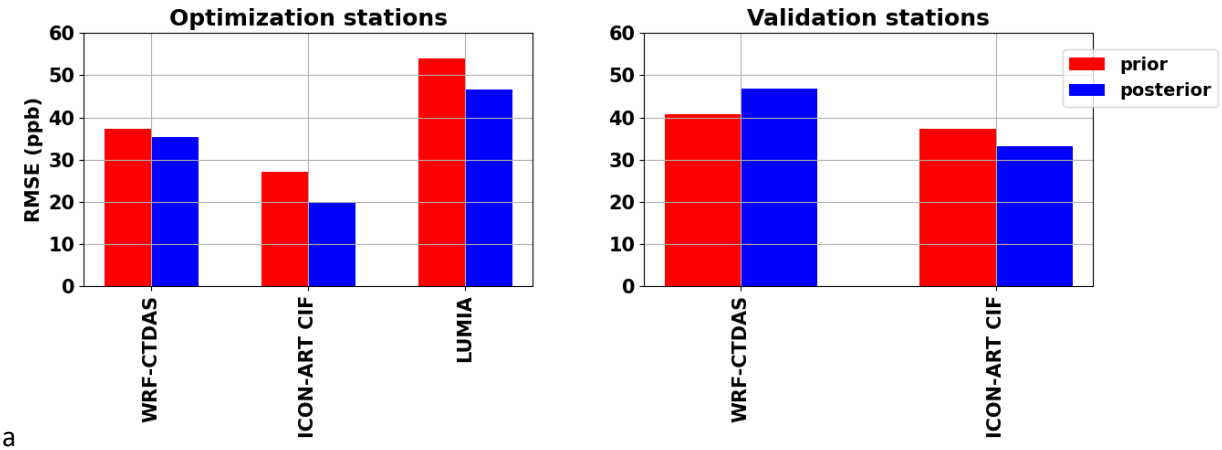
b



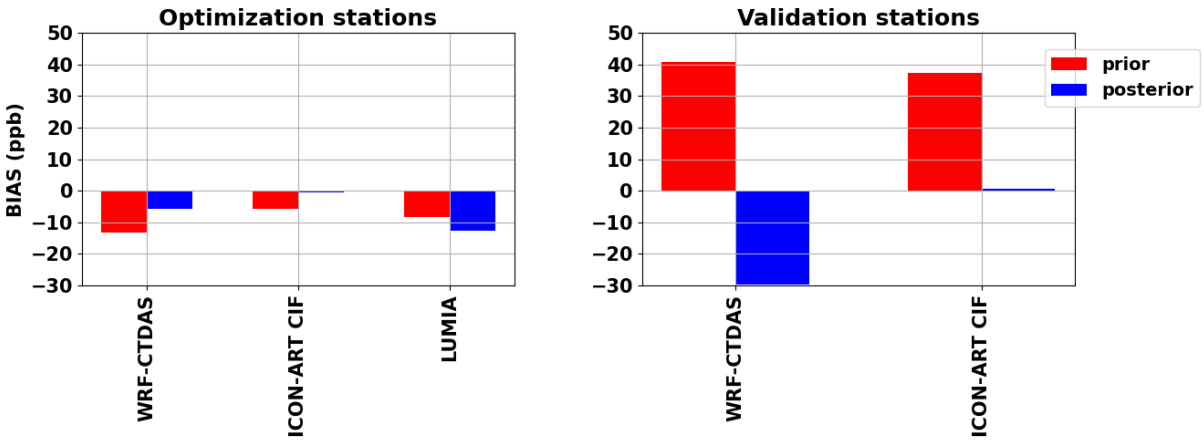
c d

Figure 5: Seasonal cycles of CH4 fluxes averaged period of 2010-2021 for the EU and Benelux areas from ICON-ART CIF(a,c) and LUMIA(b,d) after subtrating the mean.

The results so far already present some performance differences between the models. These are investigated further by comparing the root mean square error (RMSE) and the bias between model simulated mixing ratios and the observations (stations presented in Table 1) using a priori and a posteriori fluxes. The calculations were made for each station whether used in the optimization or the validation and covered the whole period. Figure 6 displays the average RMSE and BIAS from all the optimization and the validation stations separately. It is clear that the ICON-ART CIF model had the best performance with an improvement of approx. 8ppb and 3ppb for the posterior mixing ratios for the optimization and the validation stations respectively. It also showed a significant decrease of the BIAS from the prior to the posterior mixing ratios with the values going from approx. -5ppb and 38ppb to almost 0ppb for the optimization and validation stations respectively. The WRF-Chem CTDAS showed a slight decrease of approx. 1ppb for the optimization stations, but an increase of approx. 6ppb for the validation stations. This is a another indication that the WRF-Chem CTDAS optimization may remain local despite the rather large correlation and localization lengths. The bias was decreased for both the optimization and the validation stations with differences between the prior and the posterior mixing ratios 8ppb and 10ppb accordingly. Finally, the LUMIA model showed a decrease of the RMSE of approx. 8ppb, however with an increase in the bias of approx. 4ppb for the posterior mixing ratios. There were no data for the validation stations for the LUMIA model.



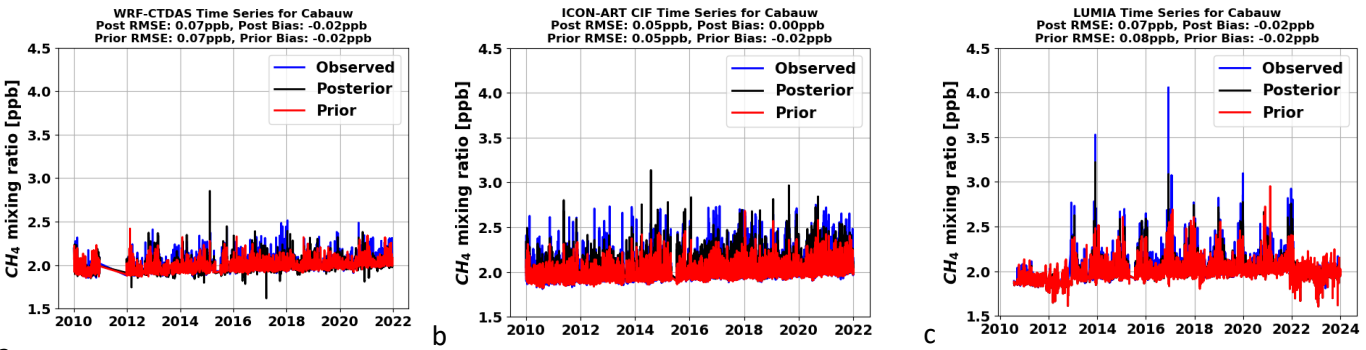
a



b

Figure 6: RMSE (a) and BIAS (b) comparisons between the mixing ratios from the WRF-Chem CTDAS, the ICON ART CIF and the LUMIA models for the prior and the posterior simulations averaged for the optimization and the validation stations separately.

Investigating further the results with regards to the mixing ratios, we present in Figure 7 the comparison between the mixing ratios of the prior and the posterior simulations alongside the observations for the stations of Cabauw and Lutjewad for the three models. This is the area where we noticed peculiar differences in the patterns, see Figure 3. All the models show an increase of approx. 0.2ppb or higher for the mixing ratios in both Cabauw and Lutjewad stations for the period 2010 to 2021. The WRF-Chem CTDAS results showed some "overcorrections" for both the Cabauw and the Lutjewad stations. In particular, for some cases, the posterior mixing ratios decrease much further than the observations reaching values below 1.7ppb in the Lutjewad station and even below 1.6ppb in the Cabauw station. Further testing needs to be made in order to detect the root of these "overcorrections". In the case of the Lutjewad station where the "overcorrections" appear more frequently, the WRF-Chem CTDAS has the highest RMSE with 0.1ppb for the prior run and 0.09 for the posterior run. Nonetheless there is an increase in BIAS from -0.01ppb for the prior run to -0.02 for the posterior run. For the Cabauw stations, the RMSE and the bias remain the same between the prior and posterior runs for the WRF-Chem CTDAS model. The ICON-ART CIF model again showcases the best performance with a decrease in the bias of approx. 0.02ppb for both stations approaching 0ppb. The RMSE remained the same (0.05ppb) for the Cabauw station and decreased for the Lutjewad station from 0.07ppb to 0.06ppb for the posterior mixing ratio. The LUMIA model displays a good performance as well with a 0.01ppb decrease of the RMSE for the posterior mixing ratios for both stations while the bias remained the same in both cases.



a b c

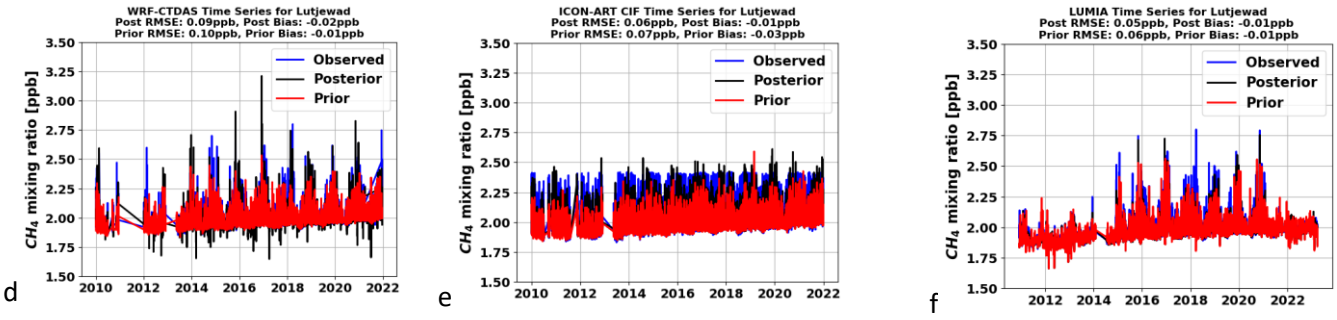


Figure 7: Ch_4 mixing ratios for the stations of Cabauw and Lutjewad for the WRF-Chem CTdas (a,d), the ICON-ART CIF (b,e) and LUMIA (c,f) with the posterior and prior RMSE and BIAS for the period 2010-2021.

6 Discussion and Conclusions

The intercomparison between the three atmospheric inversion models (WRF-Chem CTDAS, ICON-ART CIF and LUMIA) for the period 2010-2021 unfolded some interesting information regarding the CH_4 fluxes and mixing ratios in Europe. The estimation of the posterior-prior fluxes difference revealed some spatial distributions patterns over Europe. One of the most characteristic result was the positive patterns observed over the Benelux area. This was apparent especially in the ICON-ART CIF model and to a lesser extend in the LUMIA mode. The WRF-Chem CTDAS showed the positive patterns over the Cabauw and Lutjewad stations and the surrounding areas, but not in the middle of the Netherlands, indicating that the optimizations for this model might remain localized. The mixing ratios in the Cabauw and Lutjewad stations showed an increase of approx. 0.02ppb or higher for the three models.

After the validation of the models, the ICON-ART CIF model had the best performance regarding the optimization of the CH_4 fluxes. The results showed the highest decrease for both the RMSE and the bias of the posterior compared to the prior mixing ratios while being the least noisy out of the three models. More particularly, the RMSE was decreased to 8ppb and 3ppb for the optimization and the validation stations respectively. The bias reached almost 0ppb for both type of stations. For the LUMIA model, the results were more noisy, especially for the country fluxes with values varying more than 1Tgr/year between consecutive months in some cases. Nevertheles the RMSE showed a decrease of approx. 8ppb for the posterior mixing ratio, however with an incease in bias of approx. 4ppb. The validation stations results were not provided in this case. Finally, the WRF-Chem CTDAS presented the most noisy results with a slight decrease of 1ppb for the RMSE of the optimization stations and an increase of approx. 6ppb further indicating that the optimization may remain local around the stations used in the inversions. The bias decreased for the optimization station approximately for 8ppb and for the validation stations for 10ppb.

The analysis of the temporal variations for EU showed little to no enhancements for ICON-ART CIF. LUMIA and WRF-CTDAS showed large variations in the posterior fluxes with values fluctuating up to 10Tgr/year and 20Tgr/year respectively, from one month to another. All three models showed a decrease of approx. 1 to 3Tgr/year for the CH_4 fluxes in the ensemble of the European countries from January 2010 to December 2021. One of the most striking result of this analysis was the systematic enhancements observed over the Benelux area in

the ICON-ART CIF results, which as stated above had the best performance as shown by the model validation. By analysing the seasonal cycle, we found the enhancements appearing in all the twelve months. The maximum values emerged in January, February, June and July exceeding 0.6Tgr/year and the minimum values in April and May approx. 0.4Tgr/year. Overall, there seems to be a significant underestimation from the emissions inventory for Benelux.

It is also worth mentioning that for one year of the WRF-Chem CTDAS simulations presented in this study, it took more than 14 days of real time, making the use of the model very time and computationally expensive process. Further testing for the improvement of the efficiency would be very beneficial. Furthermore, WRF-Chem CTDAS simulations could be performed to test the sensitivity of the model to the correlation and localization lengths, as well as the ensemble size and see how these parameters affect the ”overcorrections” we observed. A study focusing in the Benelux area with a larger ensemble size, higher spatial and temporal resolutions is planned in Task 2.6 in order to study the different emission adjustments over the Benelux in more detail.

References

Crippa, M., Guizzardi, D., Pagani, F., Banja, M., Muntean, M., Schaaf, E., Quadrelli, R., Risquez Martin, A., Taghavi-Moharamli, P., Köykkä, J., Grassi, G., Rossi, S., Melo, J., Oom, D., Branco, A., Suárez Moreno, M., Sedano, F., San-Miguel, J., Manca, G., Pisoni, E., and Pekar, F.: GHG emissions of all world countries - 2025 Report, Publications Office of the European Union, Luxembourg, doi:10.2760/9816914, JRC143227, 2025.

Dalsøren, S. B., Myhre, C. L., Myhre, G., Gomez-Pelaez, A. J., Søvde, O. A., Isaksen, I. S. A., Weiss, R. F., and Harth, C. M.: Atmospheric methane evolution the last 40 years, Atm. Chem. Phys., 16, 3099–3126, doi:10.5194/acp-16-3099-2016, 2016.

Drell, G. A., Peckham, S E., Schmitz, R., McKeen, S. A., Frost, K., Skamarock W. C., and Eder B.: Fully coupled 'online' chemistry in the WRF model. Atmos. Environ., 39, 6957-6976, doi:10.1016/j.atmosenv.2005.04.027, 2005.

Hersbach, H., Bell, B., Berrisford, P., Biavati, G., Horányi, A., Muñoz-Sabater, J., Nicolas, J., Peubey, C., Radu, R., Rozum, I., Schepers, D., Simmons, A., Soci, C., Dee, D., Thépaut, J-N.: ERA5 hourly data on single levels from 1940 to present. Copernicus Climate Change Service (C3S) Climate Data Store (CDS), https://cds.climate.copernicus.eu/, last access: 12 January 2026.

Hersbach, H., Bell, B., Berrisford, P., Hirahara, S., Horányi, A., Muñoz-Sabater, J., Nicolas, J., Peubey, C., Radu, R., Schepers, D., Simmons, A., Soci, C., Abdalla, S., Abellan, X., Balsamo, G., Bechtold, P., Biavati, G., Bidlot, J., Bonavita, M., De Chiara, G., Dahlgren, P., Dee, D., Diamantakis, M., Dragani, R., Flemming, J., Forbes, R., Fuentes, M., Geer, A., Haimberger, L., Healy, S., Hogan, R. J., Holm, E., Janisková, M., Keeley, S., Laloyaux, P., Lopez, P., Lupu, C., Radnoti, G., de Rosnay, P., Rozum, I., Vamborg, F., Villaume, S., and Thépaut, J.-N.: The ERA5 global reanalysis, Quarterly Journal of the Royal Meteorological Society, 146, 1999–2049, doi:https://doi.org/10.1002/qj.3803, URL https://rmets.onlinelibrary.wiley.com/doi/ abs/10.1002/qj.3803, 2020.

Hoshyaripour, G. A., Baer, A., Bierbauer, S., Bruckert, J., Brunner, D., Foerstner, J., Hamzehloo, A., Hanft, V., Keller, C., Klose, M., Kumar, P., Ludwig, P., Metzner, E., Muth, L., Pauling, A., Porz, N., Reddmann, T., Reißig, L., Ruhnke, R., Satitkovitchai, K., Seifert, A., Sinnhuber, M., Steiner, M., Versick, S., Vogel, H., Weimer, M., Werchner, S., and Hoose, C.: The Atmospheric Composition Component of the ICON modeling framework: ICON-ART version 2025.04, EGUsphere, doi:10.5194/egusphere-2025-3400, URL https://doi.org/10.5194/egusphere-2025-3400, 2025, [preprint].

Ioannidis, E., Meesters, A., Steiner, M., Brunner, D., Reum, F., Pison, I., Berchet, A., Thompson, R., Sollum, E., Koch, F.-T., Wang, F., Maksyutov, S., Tenkanen, M., Aalto, T., Tsuruta, A., Monteil, G., Lin, H., Ren, G., Scholze, M., and Houweling, S.: An inter-comparison of inverse models for estimating national scale CH_4 emissions in Europe, under review in Earth System Science data, doi:10.5194/essd-2025-235, 2025.

Jackson, R. B., Saunois, M., Martinez, A., Canadell, J. G., Yu, X., Li, M., Poulter, B., Raymond, P., Regnier, P., Davis, S. J., and Patra, P.: Human activities now fuel two-thirds of global methane emissions, Environ. Res. Lett., 19, 101002, doi:10.1088/1748-9326/ad6463, 2024.

Jähn, M., Kuhlmann, G., Mu, Q., Haussaire, J.-M., Ochsner, D., Osterried, K., Clément, V., and Brunner, D.: An online emission module for atmospheric chemistry transport models: implementation in

COSMO-GHG v5.6a and COSMO-ART v5.1-3.1, Geosci. Model Dev., 13, 2379–2392, doi: 10.5194/gmd-13-2379-2020, 2020.

Kuenen, J. J. P., Visschedijk, A. J. H., Jozwicka, M., and Denier van der Gon, H. A. C.: TNO-MACC_II emission inventory; a multi-year (2003–2009) consistent high-resolution European emission inventory for air quality modelling, Atm. Chem. Phys., 14, 10963–10976, doi:10.5194/acp-14-10963-2014, 2014.

Kuenen, J., Dellaert, S., Visschedijk, A., Jalkanen, J.-P., Super, I., Denier van der Gon, H.: CAMS-REG-v4: a state-of-the-art high-resolution European emission inventory for air quality modelling. Earth Syst. Sci. Data. 14, 491–515, doi:10.5194/essd-14-491-2022, 2022.

Monteil, G. and Scholze, M.: Regional CO2 inversions with LUMIA, the Lund University Modular Inversion Algorithm, v1.0, Geosci. Model Dev., 14, 3383–3406, doi:10.5194/gmd-14-3383-2021, 2021.

Myhre, G., Shindell, D., Bréon, F.-M., Collins, W., Fuglestvedt, J., Huang, J., Koch, D., Lamarque, J.-F., Lee, D., Mendoza, B., Nakajima, T., Robock, A., Stephens, G., Takemura, T., and Zhang, H.: Anthropogenic and natural radiative forcing, in: Climate Change 2013: The Physical Science Basis. Contribution of Working Group I to the Fifth Assessment Report of the Inter- governmental Panel on Climate Change, Cambridge University Press, 659–740, doi:10.1017/CBO9781107415324.018, 2014.

Nord, J., Anthoni, P., Gregor, K., Gustafson, A., Hantson, S., Lindeskog, M., Meyer, B., Miller, P., Nieradzik, L., Olin, S., Papastefanou, P., Smith, B., Tang, J., and Wårlind, D.: LPJ-GUESS Release v4.1.1 model code, Zenodo [code], doi:10.5281/zenodo.8065737, 2021.

Peters, W., Krol, M. C., Van Der Werf, G. R., Houweling, S., Jones, C. D., Hughes, J., Schaefer, K., Masarie, K. A., Jacobson, A. R., Miller, J. B., Cho, C. H., Ramonet, M., Schmidt, M., Ciattaglia, L., Apadula, F., Heltai, D., Meinhardt, F., Di Sarra, A. G., Picentino, S., Sferlazzo, D., Aalto, T., Hatakka, J., Ström, J., Haszpra, L., Meijer, H. A. J., Var Der Laan, S., Neubert, R. E. M., Jordan, A., Rodó, X., Morguí, J.-A., Vermeulen, A. T., Popa, E., Rozanski, K., Zimnoch, M., Manning, A. C., Leuenberger, M., Uglietti, C., Dolman, A. J., Ciais, P., Heimann, M., and Tans, P. P.: Seven years of recent European net terrestrial carbon dioxide exchange constrained by atmospheric observations, Glob. Ch. Biol., 16, 1317–1337, doi:10.1111/j.1365-2486.2009.02078.x, 2010.

Prather, M. J., Holmes, C. D., and Hsu, J.: Reactive greenhouse gas scenarios: Systematic exploration of uncertainties and the role of atmospheric chemistry, Geophys. Res. Lett., 39, L09803, doi:10.1029/2012gl051440, 2012.

Randerson J., van der Werf G., Giglio L., Collatz G., Kasibhatla P.: Global Fire Emissions Database, Version 4.1 (GFEDv4). Oak Ridge Natl. Lab. Distrib. Act. Arch. Cent., Oak Ridge, TN, doi:10.3334/ORNLDAAC/1293, 2017.

Remaud, M., Chevallier, F., Maignan, F., Belviso, S., Berchet, A., Parouffe, A., Abadie, C., Bacour, C., Lennartz, S., and Peylin, P.: Plant Gross Primary Production, Plant Respiration and Car- bonyl Sulfide Emissions over the Globe Inferred by Atmospheric Inverse Modelling, Atm. Chem. Phys., 22, 2525–2552, doi:10.5194/acp-22-2525-2022, 2022.

Reum, F., Brooker, L. and Houweling, S.: Report on Level 4 performance assessment at national scale D17.1, 2021.

Rieger, D., Bangert, M., Bischoff-Gauss, I., Förstner, J., Lundgren, K., Reinert, D., Schröter J., Vogel, H., Zängl, G., Ruhnke, R., and Vogel, B.: ICON–ART 1.0 – a New Online-Coupled Model System from the Global to Regional Scale, Geo. Mod. Dev., 8, 1659–1676, doi: 10.5194/gmd-8-1659-2015, 2015.

Saunois, M., Stavert, A. R., Poulter, B., Bousquet, P., Canadell, J. G., Jackson, R. B., Raymond, P. A., Dlugokencky, E. J., Houweling, S., Patra, P. K., Ciais, P., Arora, V. K.,…, and Zhuang, Q.: The Global Methane Budget 2000–2017, Earth Syst. Sci. Data, 12, 1561–1623, doi:10.5194/essd-12-1561-2020 2020.

Savas, D., Dufour, G., Coman, A., Siour, G., Fortems-Cheiney, A., Broquet, G., Pison, I., Berchet, A., and Bessagnet, B.: Anthropogenic NOx Emission Estimations over East China for 2015 and 2019 Using OMI Satellite Observations and the New Inverse Modeling System CIF-CHIMERE, Atm., 14, 154, doi:10.3390/atmos14010154, 2023.

Shindell, D., Kuylenstierna, J. C. I., Vignati, E., van Dingenen, R., Amann, M., Klimont, Z., Anenberg, S. C., Muller, N., Janssens-Maenhout, G., Raes, F., Schwartz, J., Faluvegi, G., Pozzoli, L., Kupiainen, K., Höglund-Isaksson, L., Emberson, L., Streets, D., Ramanathan, V., Hicks, K., Oanh, N. T. K., Milly, G., Williams, M., Demkine, V., and Fowler, D.: Simultaneously Mitigating Near-Term Climate Change and Improving Human Health and Food Security, Sci., 335, 183–189, doi:10.1126/science.1210026, 2012.

Schröter, J., Rieger, D., Stassen, C., Vogel, H., Weimer, M., Werchner, S., Förstner, J., Prill, F., Reinert, D., Zängl, G., Giorgetta, M., Ruhnke, R., Vogel, B., and Braesicke, P.: ICON-ART 2.1: A Flexible Tracer Framework and Its Application for Composition Studies in Numerical Weather Forecasting and Climate Simulations, Geo. Mod. Dev., 11, 4043–4068, doi:10.5194/gmd-11-4043-2018, 2018.

Steiner, M., Peters, W., Luijkx, I., Henne, S., Chen, H., Hammer, S., and Brunner, D.: European CH_4 inversions with ICON-ART coupled to the CarbonTracker Data Assimilation Shell, Atmos. Chem. Phys., 24, 2759–2782, doi:10.5194/acp-24-2759-2024, 2024.

Szénási, B., Berchet, A., Broquet, G., Segers, A., Gon, H. D. V. D., Krol, M., Hullegie, J. J. S., Kiesow, A., Günther, D., Petrescu, A. M. R., Saunois, M., Bousquet, P., and Pison, I.: A Pragmatic Protocol for Characterising Errors in Atmospheric Inversions of Methane Emissions over Europe, Tellus B: Chemical and Physical Meteorology, 73, 1914 989, doi:10.1080/16000889.2021.1914989, 2021.

Thanwerdas, J., Saunois, M., Berchet, A., Pison, I., Vaughn, B. H., Michel, S. E., and Bousquet, P.: Variational Inverse Modeling within the Community Inversion Framework v1.1 to Assimilate $\delta^{13}C(CH_4)$ and CH_4: A Case Study with Model LMDz-SACS, Geo. Mod. Dev., 15, 4831–4851, doi:10.5194/gmd-15-4831-2022, 2022a.

Thanwerdas, J., Saunois, M., Pison, I., Hauglustaine, D., Berchet, A., Baier, B., Sweeney, C., and Bousquet, P.: How Do Cl Concentrations Matter for the Simulation of CH_4 and $\delta^{13}C(CH_4)$ and Estimation of the CH_4 Budget through Atmospheric Inversions?, Atm. Chem. and Phys., 22, 15 489–15 508, doi:10.5194/acp-22-15489-2022, 2022b.

Thanwerdas, J., Saunois, M., Berchet, A., Pison, I., and Bousquet, P.: Investigation of the Renewed Methane Growth Post-2007 with High-Resolution 3-D Variational Inverse Modeling and Isotopic Constraints, Atm. Chem. and Phys., 24, 2129–2167, doi:10.5194/acp-24-2129-2024, 2024.

Thanwerdas, J., Berchet, A., Constantin, L., Tsuruta, A., Steiner, M., Reum, F., Henne, S., and Brunner, D.: Improving the ensemble square root filter (EnSRF) in the Community Inversion Framework: a case study with ICON-ART 2024.01. Geo. Mod. Dev., 18, 1505-1544, 2025.

Wittig, S., Berchet, A., Pison, I., Saunois, M., Thanwerdas, J., Martinez, A., Paris, J.-D., Machida, T., Sasakawa, M., Worthy, D. E. J., Lan, X., Thompson, R. L., Sollum, E., and Arshinov, M.: Estimating Methane Emissions in the Arctic Nations Using Surface Observations from 2008 to 2019, Atm. Chem. Phys., 23, 6457–6485, doi:10.5194/acp-23-6457-2023, 2023.

Zängl, G., Reinert, D., Rípodas, P., and Baldauf, M.: The ICON (ICOsahedral Non-hydrostatic) Modelling Framework of DWD and MPI-M: Description of the Non-Hydrostatic Dynamical Core, Q. J. Roy. Met. Soc., 141, 563–579, doi:10.1002/qj.2378, 2015.

Appendix

Table 1: Information regarding the stations and their role to the experiment

Station	Abbreviation	Latitude	Longitude	Observation height(m)	Role	Type
Bialystok	BIK	53.2294	23.0128	273	validation	land
Birkenes	BIR	58.3886	8.2519	294	validation	land
Biscarrosse	BIS	44.3781	-1.2311	120	optimization	land
Beromunster	BRM	47.1896	8.1755	1009	optimization	mountain
Bilsdale	BSD	54.3586	-1.1504	630	optimization	land
Cabauw	CBW	51.9703	4.9264	207	optimization	land
Monte Cimone	CMN	44.1936	10.6999	2173	optimization	mountain
Centre de Recherches Atmospheriques	CRA	43.1298	0.3692	660	validation	land
Carnsore Point	CRP	52.18	-6.37	23	optimization	land
Ersa	ERS	42.9692	9.3801	573	optimization	land
Finokalia	FKL	35.3378	25.6694	265	optimization	land
Gartow	GAT	53.0657	11.4429	411	validation	land
Gredos	GIC	40.3457	-5.1755	1456	validation	mountain
Heidelberg	HEI	49.4172	8.675	143	optimization	land
Helgoland	HEL	54.1804	7.8833	153	validation	land
Heathfield	HFD	50.9767	0.2306	260	optimization	land
Hohenpeissenberg	HPB	47.8011	11.0246	1065	optimization	land
Hyltemossa	HTM	56.0976	13.4189	265	validation	land
Hegyhátsál háttérszennyettség -mérő állomás	HUN	46.9558	16.6522	363	validation	land
Ispra	IPR	45.8147	8.636	310	validation	land
Järvselja	JAR	58.2776	27.3082	146	validation	land
Jungfraujoch	JFJ	46.5475	7.9851	3585	optimization	mountain
Jülich	JUE	50.9102	6.4096	218	validation	land
Kasprowy Wierch	KAS	49.233	19.9833	1994	optimization	mountain
Karlsruhe	KIT	49.0915	8.4249	310	validation	land
Křešín u Pacova	KRE	49.572	15.08	784	validation	land
Laegern-Hochwacht	LHW	47.4822	8.3973	872	optimization	land
Lindenberg	LIN	52.1663	14.1226	171	optimization	land
Lampedusa	LMP	35.5181	12.6322	53	optimization	land
Lutjewad	LUT	53.4036	6.3528	61	optimization	land
Mace Head	MHD	53.3261	-9.9036	29	optimization	land
Malin Head	MLH	55.355	-7.333	69	optimization	land
Norunda	NOR	60.0864	17.4794	146	optimization	land
Observatoire de Haute Provence	OHP	43.931	5.712	750	optimization	land
Observatoire pérenne de l\'environnement	OPE	48.5619	5.5036	510	optimization	land
Ochsenkopf	OXK	50.03	11.8083	1185	validation	mountain

Pallas	PAL	67.9733	24.1157	577	optimization	land
Pic du Midi	PDM	42.9372	8.1411	2905	optimization	mountain
Plateau Rosa	PRS	45.93	7.7	3490	optimization	mountain
Puijo	PUI	62.9096	27.6549	316	validation	land
Puy de Dôme	PUY	45.7719	2.9658	1475	optimization	mountain
Ridge Hill	RGL	51.9975	-2.5399	297	optimization	land
Roc\'h Trédudon	ROC	48.4133	-3.8895	502	optimization	land
Saclay	SAC	48.7227	2.142	260	validation	land
Sierra de Grazalema	SGC	36.6956	-5.3975	870	validation	land
Hyytiälä	SMR	61.8474	24.2947	306	validation	land
Schauinsland	SSL	47.9167	7.9166	1217	optimization	mountain
Steinkimmen	STE	53.0431	8.4588	281	validation	land
Svartberge	SVB	64.256	19.775	419	validation	land
Tacolneston	TAC	52.5188	1.1387	249	optimization	land
Torfhaus	TOH	51.8088	10.535	948	validation	land
Trainou	TRN	47.9647	2.1125	311	optimization	land
Utö - Baltic sea	UTO	59.7839	21.3672	65	optimization	land
Valderejo	VAC	42.8786	-3.2139	1122	validation	mountain
Weybourne	WAO	52.95	1.121	41	optimization	land
Zugspitze	ZSF	47.4165	10.9796	2669	optimization	mountain

Table 2: WRF-Chem and CTDAS set-up options

Spatial resolution (km)	25x25	**Natural emissions**	GFED4.1, LPJ-GUESS, Saunois	**Scaling factors**	16158
Time step (s)	21600	**Anthropogenic Emissions**	TNO	**Region split**	2x2 grid cells
Model integration time step (s)	150	**Background/boundary conditions**	CAMS	**Correlation length (km)**	300
Vertical levels	38	**Meteorological initial/boundary conditions**	ERA5	**Localization length (km)**	900
Spectral nudging	enabled	**Assimilation time window**	20 days		

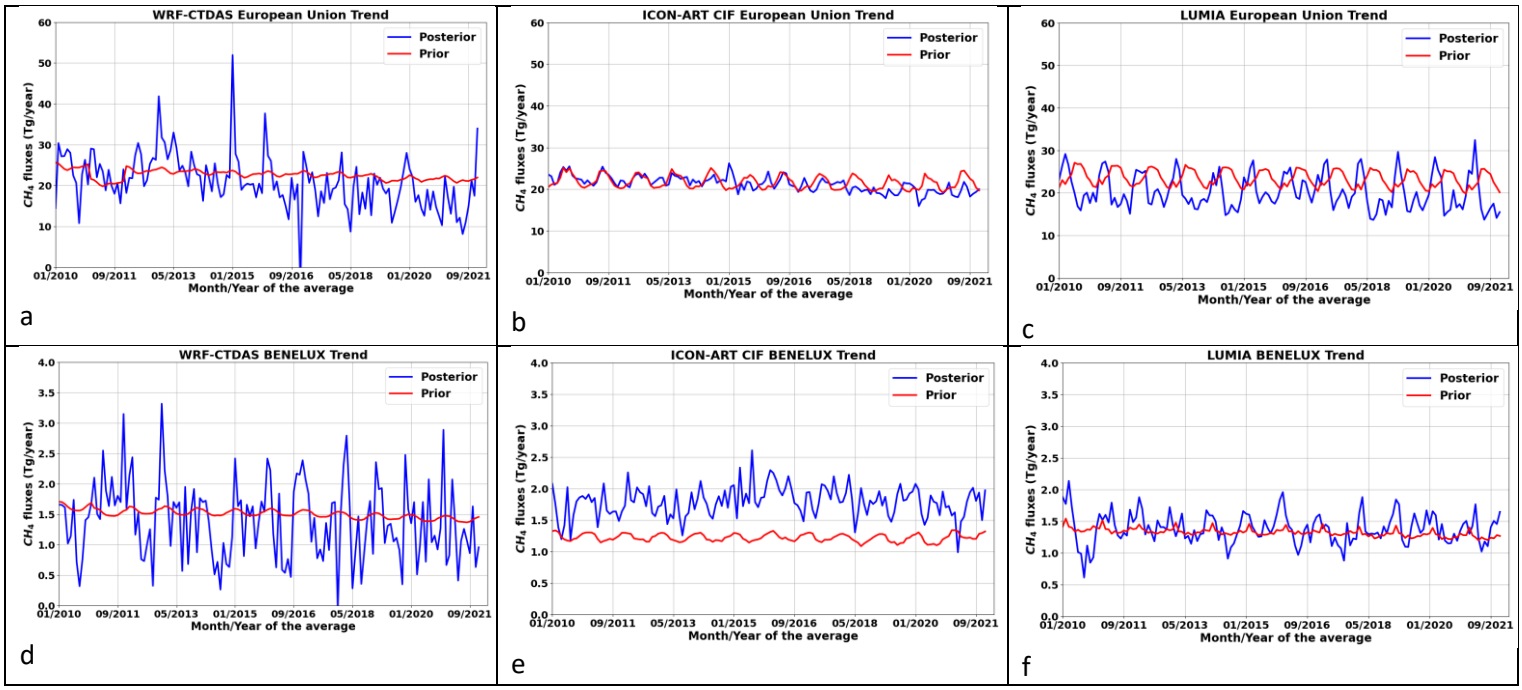


Figure 8: Monthly mean prior and posterior fluxes for the period 2010-2021 for the sum of the European Union countries (WRF-CTDAS (a), ICON-ART CIF (b) and LUMIA (c)) and the Benelux countries (WRF-CTDAS (d), ICON-ART CIF (e) and LUMIA (f)).

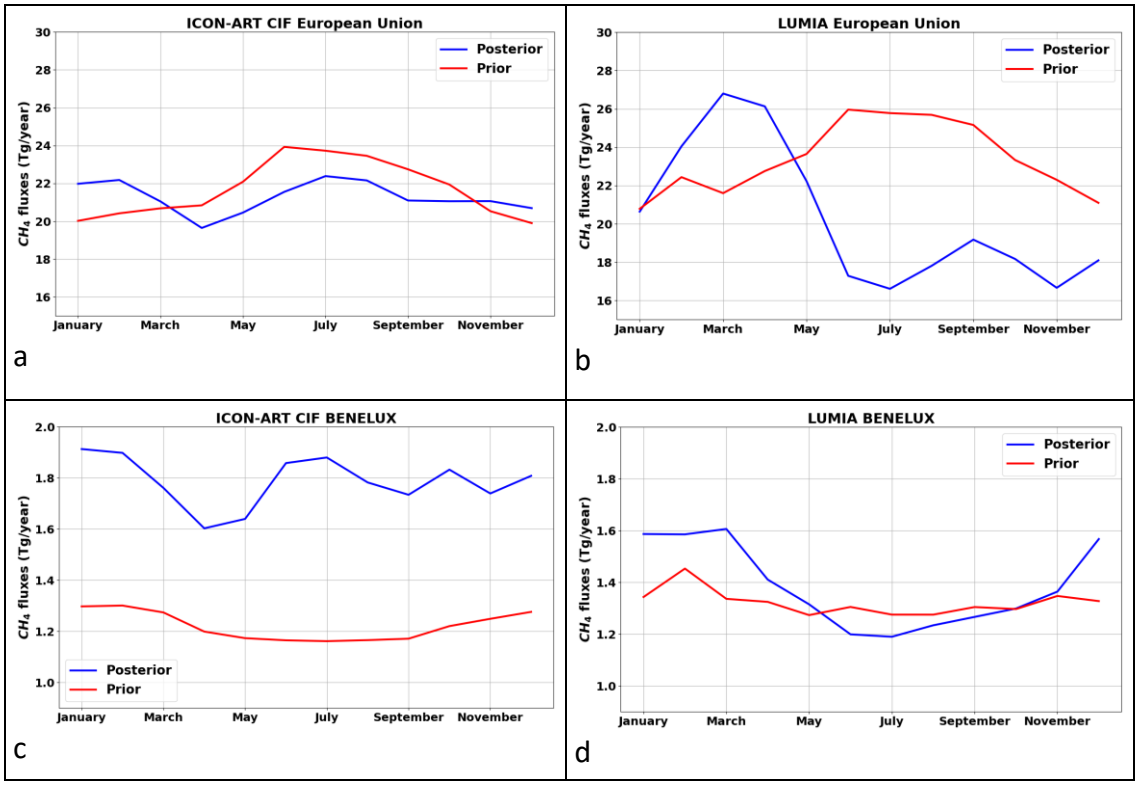


Figure 9: Figure 10: Seasonal cycles of CH4 fluxes averaged period of 2010-2021 for the EU and Benelux areas from ICON-ART CIF(a,c) and LUMIA(b,d).